Proceedings of the Korean Nuclear Spring Meeting
Gyeong ju, Korea, May 2003

Transient Multicomponent Mixture Analysis Based on ICE Numerical Technique For Simulation of an Air Ingress Accident in a HTGR

Hong Sik Lim

Korea Atomic Energy Research Institute
150 Dukjin-dong, Yuseong-gu, Teajon, Korea 305-353

Hee Cheon No

Korea Advanced Institute of Science and Technology
373-1 Guseong-dong, Yuseong-gu, Teajon, Korea 305-701

Abstract

The transient multicomponent mixture analysis tool has been developed to analyze molecular diffusion, natural convection and chemical reactions related to air ingress phenomena during the primary-pipe rupture accident of a High Temperature Gas Cooled Reactor. The present tool solves the one-dimensional basic equations for continuity, momentum, energy of the gas mixture, and mass of each species. In order to get stable and fast computation, the Implicit Continuous Eulerian scheme is adopted to solve the governing equations in a strongly coupled manner. Two kinds of benchmark calculations with Japanese inverse U-tube experiments have been performed. The present method based on the ICE technique runs faster by about 36 times for the simulation of the two experiments than the FLUENT5 does. The calculation results agree well within 10% deviations with the experimental data regarding the concentrations of gas species and the onset time of the natural circulation.

1. Introduction

A High Temperature Gas Cooled Reactor (HTGR) [1] is re-focused in nuclear field, particularly for the purpose of producing electricity as well as hydrogen for clean environment. Its achievement of very high temperature output gives a potential for this use, with high degree of passive safe performances. However, it is still unclear if the present HTGR can maintain a passive safe function during the primary-pipe rupture accident. A primary-pipe rupture accident is one of the most common of accidents related to the basic

design regarding the HTGR. It is a guillotine-type break of the main pipe of coaxial double tube at the nozzle part connecting to the bottom of the reactor vessel. When the primary-pipe rupture accident happens, one may consider that air entering into a reactor vessel reacts with high temperature graphite components and causes temperature rise of the reactor core and corrosion of graphite components. Therefore, it is very important to make sure that the air ingress accident cannot seriously oxidize the graphite fuel elements to release the radioactive materials from the reactor core to the environment nor severely damage the graphite components to loose the integrity of the reactor internals.

A schematic drawing of the HTGR, a graphite-moderated high-temperature gas-cooled thermal reactor, is shown in Figure 1. A hot leg consists of an inner passage of a coaxial duct, a high-temperature outlet duct, a high-temperature plenum and a reactor core. A cold leg consists of an annular passage of the coaxial duct, a bottom cover and an annular passage between the reactor pressure vessel and permanent reflector. When the postulated guillotine break of the coaxial pipe happens, the high-pressure helium gas is discharged into the reactor container through the breach. After a few minutes, gas pressure becomes balanced between the inside and outside of the reactor vessel. During this depressurization stage, air is unable to enter the reactor core from the breach. After the depressurization stage, it is supposed that air enters the reactor core from the breach due to molecular diffusion and weak natural convection of a multicomponent gas mixture induced by the distribution of gas temperature and the resulting concentrations in the reactor. It is possible that carbon monoxide (CO) and dioxide (CO_2) are produced in the reactor, because the oxygen (O_2) contained in air chemically reacts with the high temperature graphite structures. Density of the gas mixture in the reactor gradually increases as air enters by the molecular diffusion and weak natural convection of the gas mixture in the first stage of the accident. Finally, the second stage of the accident starts after natural circulation of the air occurs suddenly throughout the entire reactor.

This paper is concerned with development of the analysis tool to investigate the related phenomena to air ingress accident and its benchmark calculations with Japanese experiments. The following key mechanisms during the air ingress accident are considered in numerical model and discussed in the benchmark calculations: molecular diffusion in a multicomponent mixture, production/depletion of species and heat generation due to chemical reactions, and global natural circulation.

2. Governing Equations and Numerical Method

2.1 Governing Equations and Physical Models

The governing equations consist of the basic equations for continuity, momentum conservation, energy conservation of the gas mixture, and in addition mass conservation of each species. Each species equation contains the source terms to deal with molecular diffusion in a multicomponent mixture, and homogeneous and heterogeneous chemical reactions. The equation of overall continuity is obtained summing conservation equations of all gas species. The energy equation for the gas mixture includes the wall-to-fluid energy transfer term, thermal conduction term, the inter-diffusion term for energy transfer due to

molecular diffusion, and heat generation from chemical reaction. Five gas species (He, N_2, O_2, CO, CO_2) are considered in the present analytical model, and it is assumed that each gas species and the gas mixture follow the equation of state for an ideal gas. The following basic conservation equations for reacting flows are used based on Reference 2:

The equation of continuity for the gas mixture:

$$\frac{\partial r}{\partial t}+\frac{1}{A}\frac{\partial}{\partial z}(rVA)=\sum_s R_s \tag{1}$$

The equation of momentum conservation:

$$\frac{\partial}{\partial t}(rV)+\frac{1}{A}\frac{\partial}{\partial z}(rV^2A)=-\frac{\partial P}{\partial z}-rfV|V|-rg \tag{2}$$

The equation of sensible energy conservation:

$$\frac{\partial}{\partial t}(rH)+\frac{1}{A}\frac{\partial}{\partial z}(rHVA)=\frac{1}{A}\frac{\partial}{\partial z}\left(lA\frac{\partial T}{\partial z}\right)-\frac{1}{A}\frac{\partial}{\partial z}\left(A\sum_{s=1}^{m}H_sJ_s\right)-\sum_s \Delta h^o_{f_s}R_s+h(T_w-T) \tag{3}$$

The conservation equation of each species, s(s= N_2, O_2, CO, CO_2):

$$\frac{\partial}{\partial t}(rY_s)+\frac{1}{A}\frac{\partial}{\partial z}(rY_sVA)=-\frac{1}{A}\frac{\partial}{\partial z}(AJ_s)+R_s, \qquad for\ s=1\ to\ m-1,$$
$$\text{and for He,}\quad Y_m=1-\sum_{s=1}^{m-1}Y_s \tag{4}$$

The equation of state:

$$r=\frac{PW}{\bar{R}T} \quad where \quad W=\left(\sum_{s=1}^{m}Y_s/W_s\right)^{-1} \tag{5}$$

The diffusion flux (J_s) is given by two forms, full multicomponent diffusion by HCB [3] and effective diffusion [4] by assuming that a dilute species, s, diffuses through a homogeneous mixture:

$$J_s=r\frac{W_s}{W^2}\sum_{k=1,k\neq s}^{m}\left[D_{sk}\nabla(Y_kW)\right] \tag{6}$$

$$J_s=-rD_{s-mix}\nabla Y_s \quad where \quad D_{s-mix}=\left(\sum_{k=1,k\neq s}^{m}X_k/\mathbf{D}_{sk}\right)^{-1} \quad (\mathrm{m}\geq 3) \tag{7}$$

Although the full multicomponent diffusion form, Eq. (6), predicts the accurate diffusion behaviors of species in a multicomponent mixture, the effective diffusion form, Eq. (7), is generally used in numerical calculation as well as it has been investigated that the discrepancy between two diffusion forms is not so large for air diffusion through He medium in a simple vertical tube test. The friction factor and heat transfer coefficient [5] corresponding to the fully developed laminar flow are used, and the wall temperature is assumed kept constant in benchmark calculations. Physical properties, such as molar weight, viscosity, thermal conductivity, and sensible enthalpy, for each gas component and gas mixtures are obtained from Reference 4.

The most important chemical reactions between oxygen and graphite are the following heterogeneous reactions:

$C + O_2 \rightarrow CO_2 + 3.935\times10^5$ (J/mole)

$C + (1/2)O_2 \rightarrow CO + 1.105\times10^5$ (J/mole)

$C + CO_2 \rightarrow 2CO - 1.725\times10^5$ (J/mole)

and the homogeneous reaction:

$CO + (1/2)O_2 \rightarrow CO_2 + 2.830\times10^5$ (J/mole).

For the CO combustion, the reaction rate was taken from Reference 6

$$-\frac{dC_{CO}}{dt} = K_0 C_{CO} {C_{O_2}}^{1/2} {C_{H_2O}}^{1/2} \exp\left(-E_0 / \bar{R}T\right) \tag{8}$$

where $K_0 = 1.3\times10^{14}\ ml/mole\text{-sec}$ and $E_0 = 30\ kcal/mole.$

Then, a reaction rate is expressed as

$$r_{CO-O_2} = 1.3\times10^8 \exp\left(-15155.2/T\right),$$

and from Eq. (8), the dissipation/generation rates for each species are expressed as

$$R_{CO}^{\ \hom} = -r_{CO-O_2}\, r \left(\frac{r^2\times10^6}{WW_{O_2}}\right)^{0.5} Y_{CO} Y_{O_2}^{0.5} X_{H_2O}^{0.5} \quad \left[kg/m^3 - s\right] \tag{9}$$

$$R_{O_2}^{\ \hom} = -0.5 r_{CO-O_2}\, r \left(\frac{r^2\times10^6}{WW_{O_2}}\right)^{0.5} Y_{CO} Y_{O_2}^{0.5} X_{H_2O}^{0.5} \frac{W_{O_2}}{W_{CO}} \quad \left[kg/m^3 - s\right] \tag{10}$$

$$R_{CO_2}^{\ \hom} = r_{CO-O_2}\, r \left(\frac{r^2\times10^6}{WW_{O_2}}\right)^{0.5} Y_{CO} Y_{O_2}^{0.5} X_{H_2O}^{0.5} \frac{W_{CO_2}}{W_{CO}} \quad \left[kg/m^3 - s\right]. \tag{11}$$

For the graphite oxidation, the general chemical equation is expressed as

$$C + zO_2 \rightarrow xCO + yCO_2. \tag{12}$$

A reaction rate is expressed as

$$r_{C-O_2} = K_0 \exp\left(-E_0/\bar{R}T\right) {P_{O_2}}^n$$

where K_0 is the reaction constant, E_0 the activation energy and P_{O_2} the oxygen partial pressure.

Though several experiments [7, 8, 9, 10] were conducted for IG-110 nuclear-grade graphite and a few correlations [8, 11] were available in the open literatures, discrepancies among those were remarkable as shown in Figure 2. We produced a correlation based on Fuller's data [10]:

$$r_{C-O_2} = K_0 \exp\left(-188000/\bar{R}T\right)\left({P_{O_2}}^w\right)^n \quad \left[kg/m^2 - s\right]$$

where $K_0 = f(n)$ and the order of reaction (n=0.5 □ 1) is supplied by user.

A production ratio of CO and CO_2 ($x/y = f_{CO/CO_2}$) for Eq. (12) is correlated as follows:

$f_{CO/CO_2} = K_1 \exp\left(-E_1 / \bar{R}T\right)$

where $K_1 = 1995$ and $E_1 = 59860$ (Rossberg's upper curve taken from Reference 12)

Therefore, the mole number for the dissipation term of O_2 and the generation terms of CO and CO_2 can be obtained from the following relations, respectively:

$$z = \frac{f_{CO/CO_2} + 2}{2f_{CO/CO_2} + 2}, \qquad y = \frac{1}{f_{CO/CO_2} + 1}, \qquad x = \frac{f_{CO/CO_2}}{f_{CO/CO_2} + 1}$$

Then, the dissipation/generation rates for each species are expressed as

$$R_{O_2}{}^{het} = -zr_{C-O_2}\frac{W_{O_2}}{W_C}, \quad R_{CO}{}^{het} = xr_{C-O_2}\frac{W_{CO}}{W_C}, \quad \text{and } R_{CO_2}{}^{het} = yr_{C-O_2}\frac{W_{CO_2}}{W_C}. \tag{13}$$

Equation (13) is solved simultaneously with the fluid-to-surface mass transfer relationship:

$$R_s{}^{het} = r k_s \left(Y_s^w - Y_s\right), \quad for\ s = O_2,\ CO,\ CO_2 \tag{14}$$

where the mass transfer coefficient (k_s) is computed from the Sherwood number correlation, $Sh = k_s\left(d / D_{s-mix}\right) = f\left(\mathrm{Re}, Sc\right)$, and for the fully-developed laminar flow, $Sh = 3.66\left(Sc / \mathrm{Pr}\right)^{1/3}$ from heat-mass transfer analogy.

2.2 Numerical Method

As a numerical scheme, the Implicit Continuous Eulerian (ICE) scheme [13] is adopted for fast computation. The governing equations are discretized in a semi-implicit manner in the staggered mesh layout and then dependent variables are linearized by the Newton Raphson method. In a staggered spatial nodding, the mesh cell configuration is:

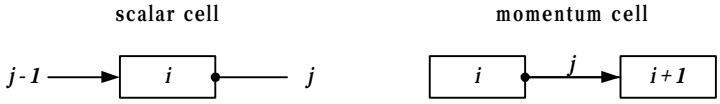

where i is the index of scalar cell and j the index of momentum cell. A combination of circle and arrow indicates the flow direction from the upstream node to the downstream node.

In the ICE scheme, since the equation of momentum conservation should be expressed as a function of pressure only, the non-conservative form of Eq. (2) is used as

$$\frac{\partial V}{\partial t} + V\frac{\partial V}{\partial z} = -\frac{1}{r}\frac{\partial P}{\partial z} - g - fV|V|. \tag{15}$$

Then, all conservation equations, Eqs. (1), (3), (4), and (15), are discretized as follows:

$$\frac{r_i^{n+1} - r_i^n}{\Delta t} + \frac{1}{Vol_i}\left(\dot{r}_j{}^n A_j V_j^{n+1} - \dot{r}_{j-1}{}^n A_{j-1} V_{j-1}{}^{n+1}\right) = \sum_s R_{s\,i}{}^{n+1} \tag{16}$$

$$\frac{(V)_j^{n+1} - (V)_j^n}{\Delta t} + V_j^n \frac{\dot{V}_{i+1}{}^n - \dot{V}_i^n}{\Delta z_j} = -\frac{\left(P_{i+1} - P_i\right)^{n+1}}{\bar{r}_j{}^n \Delta z_j} - f_j^n \left(V^2\right)_j^{n+1} - g_j^n \tag{17}$$

$$\frac{(rH)_i^{n+1}-(rH)_i^n}{\Delta t}+\frac{1}{Vol_i}\left(\dot{r}_j^{\,n}\dot{H}_j^n A_j V_j^{\,n+1}-\dot{r}_{j-1}^{\,n}\dot{H}_{j-1}^n A_{j-1}V_{j-1}^{\,n+1}\right)=-\sum_s \Delta h_{f_s}^o R_{si}^{\,n+1}+h_i^n\left(T_{wi}^{\,n}-T_i^{n+1}\right)$$
$$+\frac{1}{Vol_i}\left(\bar{l}_j^{\,n}A_j\frac{T_{i+1}^{\,n}-T_i^n}{\Delta z_j}-\bar{l}_{j-1}^{\,n}A_{j-1}\frac{T_i^n-T_{i-1}^{\,n}}{\Delta z_{j-1}}\right)-\frac{1}{Vol_i}\left[A_j\sum_{s=1}^m\left(\overline{H}_{sj}^{\,n}J_{sj}^{\,n}\right)-A_{j-1}\sum_{s=1}^m\left(\overline{H}_{sj-1}^{\,n}J_{sj-1}^{\,n}\right)\right] \tag{18}$$

$$\frac{(rY_s)_i^{n+1}-(rY_s)_i^n}{\Delta t}+\frac{1}{Vol_i}\left(\dot{r}_j^{\,n}\dot{Y}_{sj}^{\,n}A_j V_j^{\,n+1}-\dot{r}_{j-1}^{\,n}\dot{Y}_{sj-1}^{\,n}A_{j-1}V_{j-1}^{\,n+1}\right)=-\frac{1}{Vol_i}\left(A_j J_{sj}^{\,n}-J_{sj-1}^{\,n}A_{j-1}\right)+R_{si}^{\,n+1} \tag{19}$$

where bar(-) indicates average properties and dot(·) indicates donor properties which depend on flow direction.

By the Newton method, pressure is linearized as $P^{n+1}\rightarrow P^k+dP$ and then inserted into Eq. (17), eventually resulting in the following form:

$$V_j^{\,n+1}=V_j^{\,k}+Jacob_j\left(dP_i-dP_{i+1}\right)$$
$$where\quad Jacob_j=\frac{\Delta t}{\bar{r}_j^n\Delta z_j\left(1+\Delta t 2f_j^n|V_j^n|\right)} \tag{20}$$
$$V_j^{\,k}=\frac{V_j^n-\Delta t\left[V_j^n\frac{\dot{V}_{i+1}^{\,n}-\dot{V}_i^n}{\Delta z_j}-f_j^n V_j^n|V_j^n|+\frac{\left(P_{i+1}^k-P_i^k\right)}{\bar{r}_j^n\Delta z_j}+g_j^n\right]}{1+\Delta t 2f_j^n|V_j^n|}$$

Also, other dependent variables (r , Y_s, T, H) and source terms are linearized as follows:

$$Y_s^{n+1}\rightarrow Y_s^k+dY_s,\quad T^{n+1}\rightarrow T^k+dT$$
$$r^{n+1}\rightarrow r^k+\left(\frac{\partial r}{\partial P}\right)^k dP+\left(\frac{\partial r}{\partial T}\right)^k dT+\sum_s\left(\frac{\partial r}{\partial Y_s}\right)^k dY_s$$
$$H^{n+1}\rightarrow H^k+\left(\frac{\partial H}{\partial T}\right)^k dT+\sum_s\left(\frac{\partial H}{\partial Y_s}\right)^k dY_s \tag{21}$$
$$R_s^{\,n+1}\rightarrow R_s^{\,k}+\sum_s\left(\frac{\partial R_s}{\partial Y_s}\right)^k dY_s$$

By inserting $V_j^{\,n+1}$ of Eq. (20) and linearized variables of Eq. (21) into discretized scalar equations, Eqs. (16), (18), and (19), and then combining the resulting equations into linear algebraic form, the 6×6 square matrix is obtained:

$$\underline{\underline{B}}\,d\underline{X}=\underline{b}+\underline{c}\left(dP_{i+1}-dP_i\right)-\underline{d}\left(dP_i-dP_{i-1}\right)$$
$$where\quad \left[dX\right]^T=\left[dP\quad dT\quad dY_{N_2}\quad dY_{O_2}\quad dY_{CO}\quad dY_{CO_2}\right]^T \tag{22}$$

Multiplying Eq. (22) by the inverse matrix ($\underline{\underline{B}}^{-1}$), the solution vector is expressed as

$$d\underline{X}=\underline{\underline{B}}^{-1}\underline{b}+\underline{\underline{B}}^{-1}\underline{c}\left(dP_{i+1}-dP_i\right)-\underline{\underline{B}}^{-1}\underline{d}\left(dP_i-dP_{i-1}\right). \tag{23}$$

As a result, the first row in Eq. (23) becomes N×N pressure matrix and this pressure matrix is solved by the direct method using Gauss elimination [14]. The remaining rows in Eq. (23), temperature and mass fraction of each species, are simply expressed as a function of pressure only. As shown in Figure 3, the above calculation processes are repeated until the convergence criterion, $e = \max\left(d P_i / P_i^k\right)$, is satisfied. According to the condition under which the convergence succeeds or fails, the time step is controlled but restricted by the time step limit due to explicit treatment of the second-order terms, that is,

$$\Delta t_{\max} \le \min\left(\Delta t_{convective},\ \Delta t_{conductive},\ \Delta t_{diffusive}\right).$$

3. Benchmark Calculations

3.1 Benchmarks for Inverse U-tube Experiments

Figures 4 and 5 show the test apparatus [15] to investigate molecular diffusion behavior in binary mixture and the nodalization diagram for the present model, respectively. The apparatus consists of an inverse U-shaped tube having an inner diameter of 52.7 mm and a gas tank. The ball valves between the reverse U-tube and the gas tank were closed and the tube was evacuated by a vacuum pump. Helium and nitrogen are filled in the tube and the gas tank, respectively. Then, the high temperature side and connecting pipes were heated to elevated temperatures. When the temperature of the gas and the pipe wall reached a steady state condition, the gas pressure in the reverse U-tube was equalized to the atmosphere pressure by opening a small release valve.

When the valves open simultaneously, N_2 gas in the bottom tank starts to diffuse into both sides of the inverse tube. Two kinds of experiments were performed: isothermal test and non-isothermal test. In the isothermal test the inverse U-tube is kept at room temperature (18^{o}C). In the non-isothermal test the inverse U-tube has non-uniform temperature distribution along the tube: 19.3^{o}C in the hot side cooler, 256^{o}C in the lower part of hot side, 154^{o}C in the upper part of hot side, 124^{o}C in the horizontal pipe, 59^{o}C in the upper of cold side, 26.3^{o}C in the lower part of cold side, 17.7^{o}C in the cold side cooler, 18^{o}C in the bottom tank. The mole fraction of N_2 was obtained at eight sampling points (C-1 through C-4 and H-1 through H-4) shown in Figure 4 by measuring the sound velocity of the gas mixture.

3.1.1 Isothermal Test

When valves in both sides open, N_2 in a gas tank begins to move into the inverse tube filled with He by pure molecular diffusion. As mole fraction distribution of N_2 is the same between the hot and cold pipes, natural convection of the gas mixture does not occur. As shown in Figure 6, the calculated results agree well within 10% deviation with the experimental ones. A slight discrepancy with the experiment seems to be caused by the entrance effect at the tube inlet, that is, non-uniform concentration distribution.

3.1.2 Non-isothermal Test

The calculated results using non-uniform temperature distribution are shown in Figures 7

and 8. As the mole fraction of N_2 in the tube gradually increases, the buoyancy force induced by the distribution of the gas mixture density increases. Around 220 minutes after the valves open, the buoyancy force becomes large enough to initiate global natural circulation throughout the inverse U-tube. The calculated velocities by very weak and global natural convection are about $< 10^{-4}$ m/s in the early stage and around 1 m/s (Re_d =500) in the later stage, respectively. The predicted results agree well within 10% deviation with the experimental values measured at six sampling locations. In particular, although the trends of mole fractions of N_2 with respect to time are a little different, the onset time of natural convection is almost the same. As observed in the isothermal test, the slight discrepancy of mole fractions of N_2 is attributed to the entrance effect between the tube inlet and the gas tank and the use of rough temperature distribution along the tube.

3.1.3 Comparisons with FLUENT simulations

Figures 6 through 8 also show comparative results between the present calculations and FLUENT simulations for both isothermal and non-isothermal tests. The FLUENT5 [16] simulations are performed with the SIMPLE algorithm using the 3-D mesh layout in Figure 9. To reduce the computation time, the original circular geometry of the test apparatus was transformed into the rectangular shape for generating coarse meshes by preserving the volumes of the bottom tank and the connecting pipe. The predicted trends are very similar in both FLUENT and the present model. The remarkable one is the comparison of their computing times given in Table 1. Even though the number of mesh used in the FLUENT calculation is about twice more than that in the present model, it takes very long time in the FLUENT calculation, almost 40 times more than that of the present model. In addition, the maximum time step is restricted to be lower than that of the present model.

3.2 Benchmark for Inverse U-tube Experiment with a Graphite Tube

Figures 10 and 11 show the experimental apparatus [11] consisting of a gas tank and an inverse U-shaped tube with a graphite (IG-110) tube inserted at the middle of hot side and the nodalization diagram of the present model. The experimental procedure was the same as that described in Section 3.1, except that air instead of N_2 was filled in the gas tank. The mole fraction of each gas species and the density of the gas mixture were measured at four sampling points shown in Figure 10 using a gas analyzer (Yokogawa: density-Vibro gas analyzer DG8, O_2-electrochemical analyzer 6234, CO and CO_2-infrared rays analyzer IR21).

When the ball valves open, air enters into the vertical pipe by molecular diffusion and weak natural convection, and then chemically reacts with the graphite. As the graphite is oxidized by chemical reaction with oxygen, CO and CO_2 are produced and transported both upward and downward. A part of CO produced dissipates by homogeneous reaction with oxygen, and also a part of CO_2 produced dissipates by reverse reaction (Boudouard reaction) at very high temperature. As time passes, the density of gas mixture in the hot side increases gradually, and eventually global natural convection occurs. During the transient calculation, the non-uniform wall temperature distribution along the pipe shown in Figure 12 is assumed kept constant. The CO_2 reverse reaction is not considered in the present calculation because graphite temperature is relatively low, less than 850^{o}C.

Figures 13 through 16 show the predicted results of the densities of gas mixture and mole fractions of O_2, CO, and CO_2 at different sampling locations. As shown in Figure 13, as N_2 and O_2 in the gas tank are transported into the tube and CO and CO_2 are produced by chemical reaction with the graphite, the buoyancy force induced by the distribution of the gas mixture density gradually increases. Around 100 minutes after the valves open, the buoyancy force becomes large enough to initiate global natural circulation throughout the inverse U-tube. The calculated velocities by very weak and global natural convection are about $< 3\times10^{-4}$ m/s in the early stage and around 0.2 m/s (Re_d =400) in the later stage, respectively. The range of the Rayleigh number calculated based on the height of the inverse U-tube is about $1\times10^9 < Ra_H < 5\times10^{10}$. The calculated O_2 mole fractions in both cold and hot sides are higher than the experimental ones, as shown in Figure 14. It seems to be caused by the entrance effect at the tube inlet, as observed in the non-isothermal test. The calculated CO_2 and CO mole fractions shown in Figures 15 and 16 are a little different from those of the measured ones. Even with some discrepancies in the concentrations of species, the onset time of natural convection agrees well with that of the experiment because the density change of the gas mixture is less sensitive to the concentrations of species.

In the present calculation, a value of 0.5 has been used for the order of the reaction (n) in the graphite oxidation correlation. Since the oxygen transported from the bottom tank is completely consumed within one-third portion from the inlet of the graphite tube, the surface reaction rate is mostly "chemically-controlled" and in this situation the order of the reaction of 0.5 is appropriate. A higher value of the order of reaction is appropriate when the surface reaction rate is mostly "mass transport-controlled." To get the prediction results for CO mole fractions of Figure 16, a small mole fraction of 0.5×10^{-6} has been used for X_{H_2O} in the CO combustion correlation without evident basis because the effect of moisture on CO combustion is still uncertain.

4. Conclusions

In the benchmark calculations with the inverse U-tube experiments for both isothermal and non-isothermal tests, the difference between the predicted results and the experimental data is within 10% deviation regarding the concentrations of species and the onset time of the natural circulation. As well, the calculation results of the present model are almost identical with those of the FLUENT5 simulations and the present model runs faster by about 36 times than the FLUENT5 does, in a 900 MHz Pentium III PC.

In the benchmark calculation for the inverse U-tube experiment with a graphite specimen, the prediction results agree well within 10% deviation with the experimental data. To justify selected values for the order of the reaction for the graphite oxidation and the initial mole fraction of moisture for the CO combustion, further investigations are necessary because there are few experimental works on the effects of these parameters.

References

[1] HTR-TN 2002 1st international Topical Meeting on High Temperature Reactor

Technology (HTR), Petten, The Netherlands, April 22-24, 2002.
[2] T. Poinsot and D. Veynante, Theoretical and Numerical Combustion, 2001, R.T. Edwards, Inc.
[3] J.O. Hirschfelder, C.F. Curtiss, and R.B. Bird, Molecular Theory of Gases and Liquids, 2nd Edition, 1964, Wiley.
[4] B.E. Poling, J.M. Prausnitz, and J.P. O' connell, The Properties of Gases and Liquids, 5th Edition, 2001, McGraw-Hill.
[5] R.B. Bird, W.E. Stewart, and E.H. Lightfoot, Transport Phenomena, 2nd Edition, 2002, John Wiley & Sons.
[6] J. B. Howard, G. C. Williams, and D.H. Fine "Kinetics of carbon monoxide oxidation in postflame gases," 14th symposium (international) on combustion, pp.975-986, 1973.
[7] H. Kawakami, "Air oxidation behavior of carbon and graphite materials for HTGR," TANSO 124, pp. 26-33, 1986.
[8] M. Ogawa, "Mass transfer with graphite oxidation in gas mixture laminar flow through circular tube," J. At. Energy Soc. Jpn., Vol. 35, No. 3, p. 245, 1993.
[9] M. Takahashi, M. Kotaka, and H. Sekimoto, "Burn-off and production of CO and CO_2 in the oxidation of nuclear reactor-grade graphites in a flow system," J. Nucl. Sci. Tech., Vol.31, No.12, pp.1275-1286, December 1994.
[10] E. L. Fuller and J. M. Okoh, "Kinetics mechanisms of the reaction of air with nuclear grade graphites: IG-110," J. Nuclear Materials, Vol.240, pp. 241-250, 1997.
[11] T. Takeda and M. Hishida, "Studies on molecular diffusion and natural convection in a multicomponent gas system," Int. J. Heat Mass Transfer, Vol.39, No.3, pp.527-536, 1996.
[12] M.Rossberg, Z. Elektrochem. 60, p.952, 1956.
[13] F.H. Harlow and A.A. Amsden, " A numerical fluid dynamics calculation method for all flow speeds," J. Comp. Phy., Vol.8, pp.197-213, 1971.
[14] S. Nakamura, Applied Numerical Methods in C, 1995, Prentice-Hall.
[15] M. Hishida and T. Takeda, "Study on air ingress during an early stage of a primary-pipe rupture accident of a high-temperature gas-cooled reactor", Nucl. Eng. & Des. 126 (1991) 175-187.
[16] FLUENT5 User's Guide, July 1998.

Nomenclature

A = cross-sectional flow area (m^2)
C_s = concentration of species s
d = hydraulic diameter (m)
D_{sk} = multicomponent diffusion coefficient (m^2/s)
$\mathbf{D}_{sk}$ = binary diffusion coefficient (m^2/s)
D_{s-mix} = effective diffusion coefficient (m^2/s)
f = friction factor
f_{CO/CO_2} = production ratio of CO and CO_2 for graphite oxidation
g = gravitational constant
h = wall-to-fluid heat transfer coefficient (W/m^2-K)

Δh_f^o = latent heat of formation for chemical reaction (J/kg)
H = sensible enthalpy of gas mixture (J/kg)
H_s = sensible enthalpy of species s (s=He, N_2, O_2, CO, CO_2) (J/kg)
J_s = total diffusion flux with respect to mass average velocity (kg/m^2-s)
k_s = mass transfer coefficient of species s (m/s)
m = total number of species
N = total number of scalar nodes or cells
P = total pressure (Pa)
P_{O_2} = oxygen partial pressure (Pa) in the bulk, and $P_{O_2}^{w}$ at the surface of the wall
$\overline{R}$ = universal gas constant
R_s = generation/dissipation of species s by chemical reaction (kg/m^3-s)
t = time (sec)
T = temperature of gas mixture (K)
T_w = wall temperature (K)
V = mass average velocity of gas mixture (m/s)
Vol = fluid volume (m^3)
X_s = mole fraction of species s
Y_s = mass fraction of species s in the bulk, and Y_s^w at the surface of the wall
W = molar weight of gas mixture (g/mol)
W_s = molar weight of species s (g/mol)
W_C = molar weight of graphite (g/mol)
z = spatial coordinate
e = convergence criterion
l = thermal conductivity of gas mixture (W/m-K)
r = density of gas mixture (kg/m^3)
Ra = Rayleigh number
Re = Reynolds number
Nu = Nusselt number
Sc = Schmidt number
Sh = Sherwood number

Table 1 Computation times and time steps for ICE and FLUENT

Test cases	Max. time step		Computation time		Time step limit
	ICE	FLUENT	ICE	FLUENT	-
Isothermal	0.5 sec	0.2 sec	32 min.	20 hrs	4.7 sec (diffusion)
Non-isothermal	0.5 sec	0.2 sec	36 min.	22 hrs	0.6-1.7 sec (conduction)

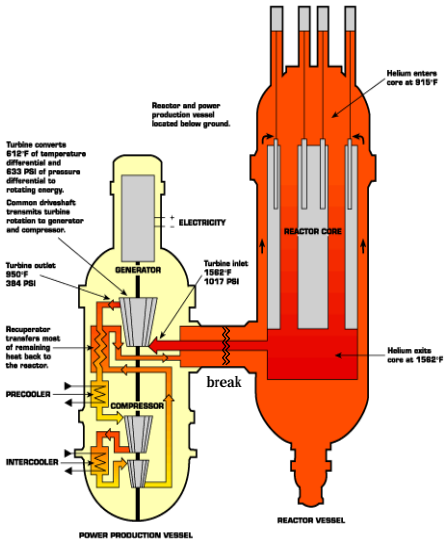

Fig. 1 Schematic diagram of a HTGR

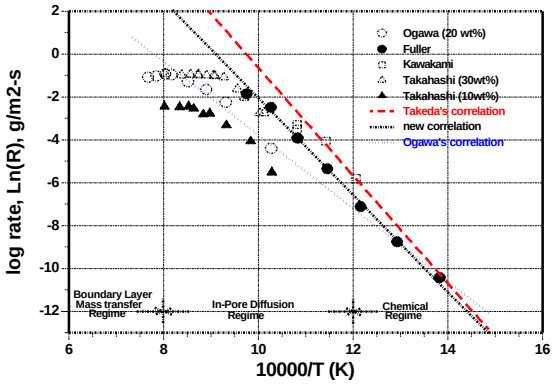

Fig. 2 Oxidation data and correlations for IG-110

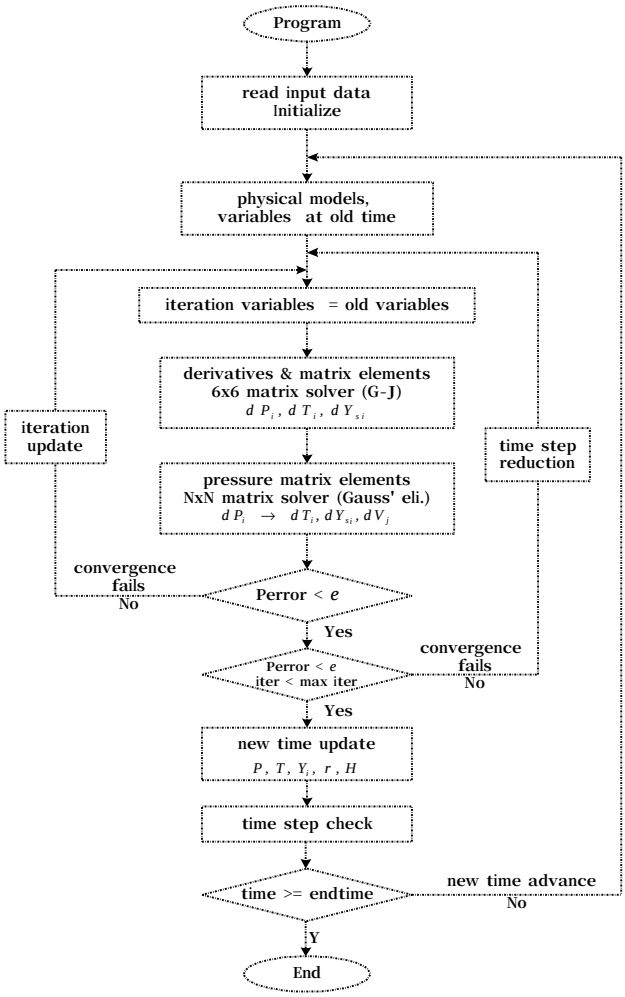

Fig. 3 Calculation procedure of the present model

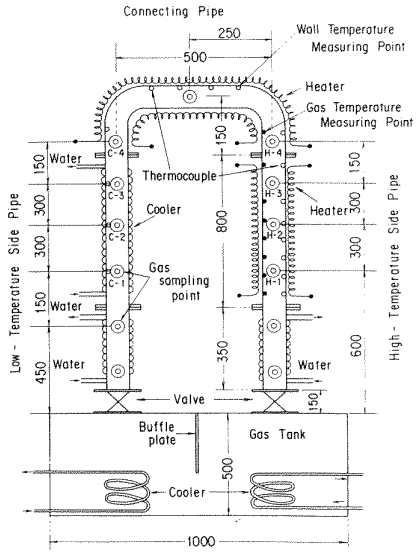

Fig. 4 Inverse U-tube experimental apparatus

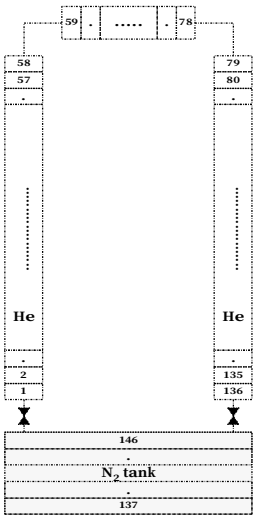

Fig. 5 Nodalization diagram for the inverse U-tube experimental apparatus

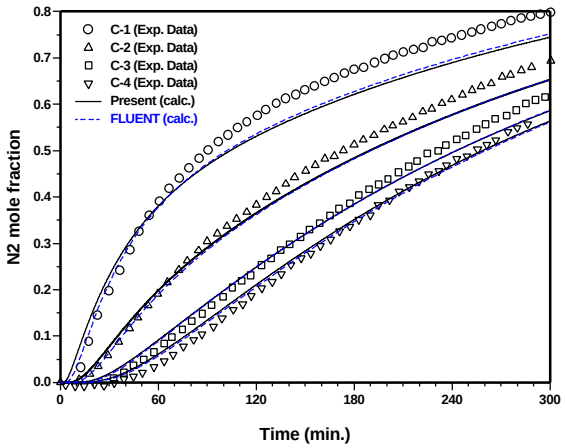

Fig. 6 N_2 mole fraction (isothermal test)

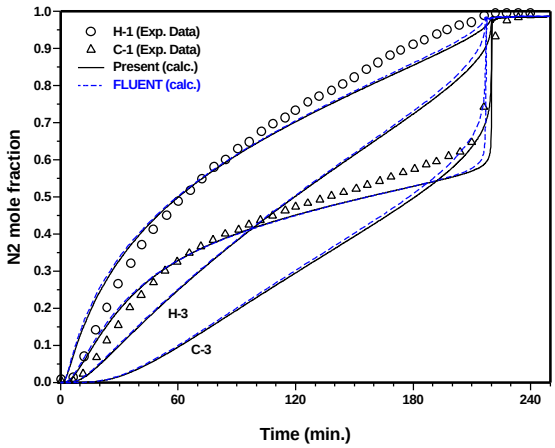

Fig. 7 N_2 mole fraction (non-isothermal test)

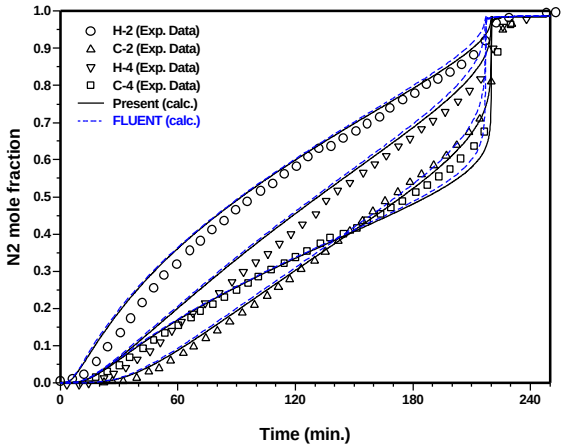

Fig. 8 N_2 mole fraction (non-isothermal test)

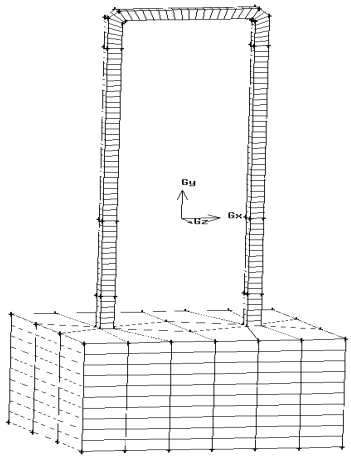

Fig. 9 FLUENT5 mesh layout for test apparatus

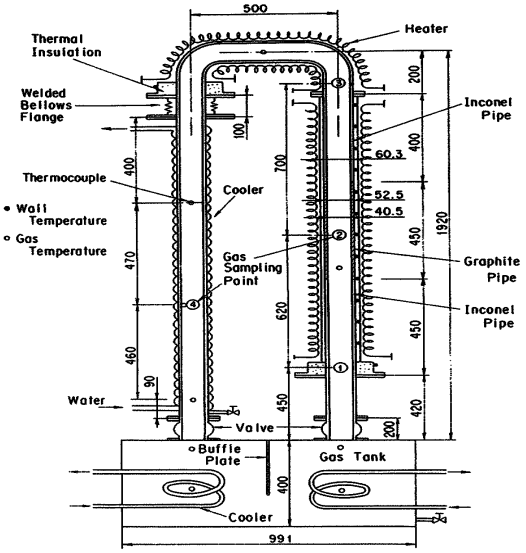

Fig. 10 Experimental apparatus with a graphite tube

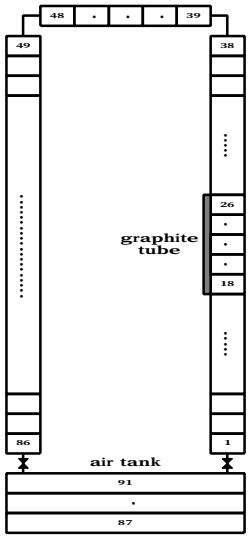

Fig. 11 Nodalization diagram for test apparatus with a graphite tube

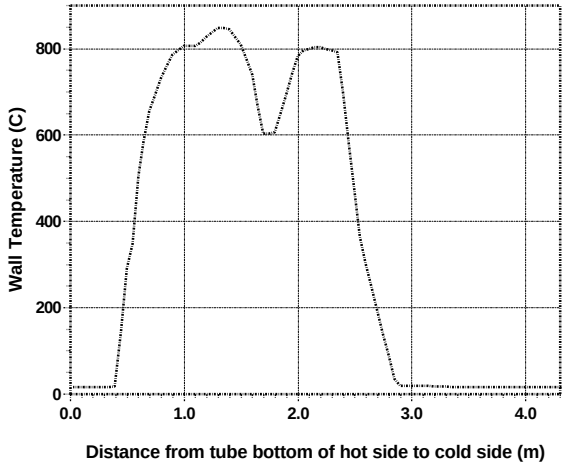

Fig. 12 Non-uniform temperature distribution along the inverse U-tube

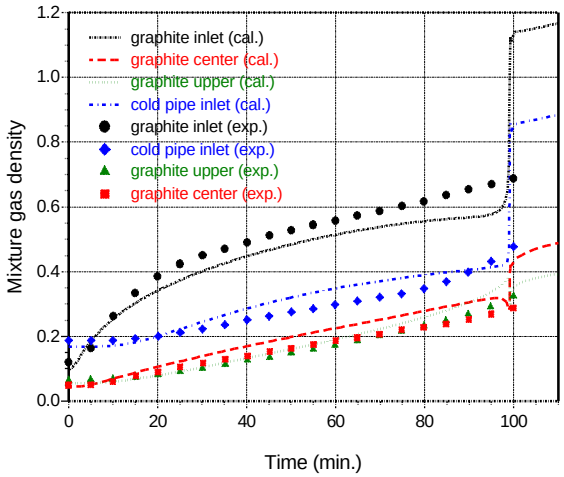

Fig. 13 Predictions of density of a gas mixture

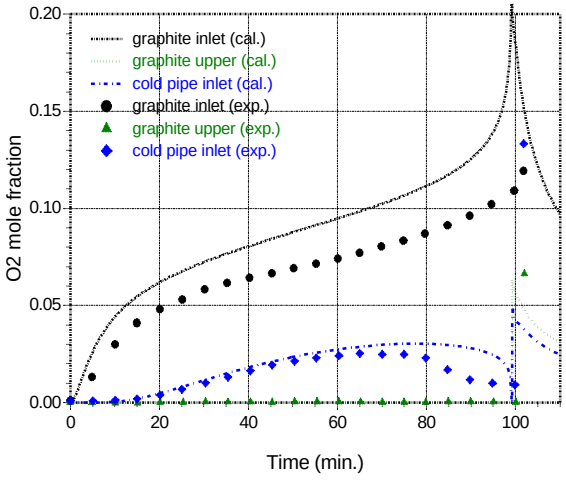

Fig. 14 Predictions of O_2 mole fraction

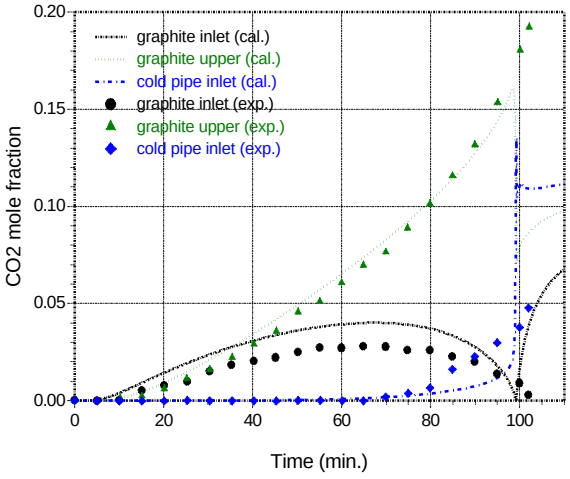

Fig. 15 Predictions of CO_2 mole fraction

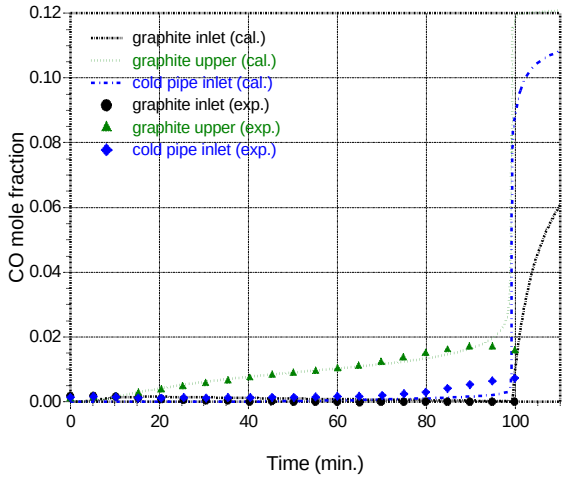

Fig. 16 Predictions of CO mole fraction